# Optical setup for Rydberg excitation of Rubidium

Teresa Grafen

# Bachelorarbeit in Physik angefertigt im Institut für Angewandte Physik

vorgelegt der Mathematisch-Naturwissenschaftlichen Fakultät der Rheinischen Friedrich-Wilhelms-Universität Bonn

July 2025

Ich versichere, dass ich diese Arbeit selbstständig verfasst und keine anderen als die angegebenen Quellen
und Hilfsmittel benutzt sowie die Zitate kenntlich gemacht habe.  Bonn, 30.07.2025
Datum Unterschrift
1. Gutachter: Prof. Dr. Sebastian Hofferberth

2. Gutachter: Prof. Dr. Stefan Linden

# **Acknowledgements**

I would like thank Prof. Hofferberth for giving me the opportunity to write my Bachelor thesis in the NQO group. I am also thankful to Prof. Linden for kindly agreeing to serve as my second supervisor. A special thanks goes to all members of the HQO lab for their support, helpful feedback, and the collaborative atmosphere. Working on this thesis has been a truly rewarding experience, and I'm grateful for everything I've learned along the way.

# **Contents**

1	Intro	oduction	1	
2	Lase	er system for Rydberg excitation	2	
	2.1	Rydberg-states	3	
	2.2	Requirements for Rydberg excitation	4	
3	Setup of Rydberg control laser 6			
	3.1	Acoustic optical modulator setup	8	
		3.1.1 AOM driver box	9	
		3.1.2 Telescope	9	
		3.1.3 AOM response curve	10	
	3.2	Mechanical shutter	11	
	3.3	Fibre coupling and polarisation	13	
4	Rydberg excitation measurements 15			
	4.1	Atom preparation and characterisation	16	
	4.2	Rydberg excitation and detection	17	
		4.2.1 Detuning of Rydberg control laser	17	
		4.2.2 Alignment of probe and Rydberg control laser	19	
		4.2.3 Measurement of Rydberg signal in single photon regime	21	
5	Con	clusion and Outlook	23	
A	App	endix	25	
	<b>A.</b> 1	Pound-Drever-Hall Method	25	
Bil	bliogr	aphy	26	

### Introduction

In recent years, there has been an increase of interest in the field of quantum technology [1]. This has had a significant impact on quantum computing and nonlinear quantum optics, among other fields [2]. Superconducting qubits and Rydberg atoms are two out of multiple promising platforms for quantum computing [3, 4]. When combined, they form a hybrid system that benefits from the advantages of both systems [5]. Rydberg atoms are highly excited atoms with transitions covering a broad range of the electromagnetic spectrum [4]. The coupling between the ground and the Rydberg state can be achieved optically, while transitions between neighbouring Rydberg states are located in the microwave regime [6]. This makes Rydberg atoms especially interesting for hybrid systems. This property can be used in an experiment, where a connection between different frequency regimes can be established. These systems can for example be utilised for further research on quantum information transfer in different frequency regimes [5].

In the Hybrid Quantum Optics lab of the Nonlinear Quantum Optics group, the goal is to interface Rydberg atoms with an electromagnetic oscillator in the GHz regime. This system is tackled from two sides: the Rydberg atom side and the electromagnetic oscillator side.

The experimental setup contains the magneto-optical trap chamber, where the preparation of cold atoms takes place. Thereafter, they are magnetically transported to the science chamber, where the rubidium atoms are excited to the Rydberg state and later the interaction with the electromagnetic oscillator will be implemented.

This thesis focuses on the Rydberg atom part of the experiment and in more detail on the second Rydberg control laser setup. This setup provides a control beam, which is focussed on the rubidium atoms in the science chamber and co-propagating to the probe beam. The structure of this thesis is as follows. In Chapter 2 the laser system that is required for Rydberg excitation will be depicted, including the definition of Rydberg atoms and the requirements for Rydberg excitation. In the following Chapter 3, the setup of the Rydberg control laser is explained, including characterisation and optimisation of optics to be able to prepare the light for the Rydberg excitation. In Chapter 4, an overview of the cold atom preparation of the rubidium atoms is presented. Then, the implementation of the control laser around the science chamber is described, where the adjustment of the wavelength and the detuning of the Rydberg control laser are discussed. Finally, first measurements of Rydberg signals in the single photon regime, using the newly implemented control laser, are outlined.

### Laser system for Rydberg excitation

In order to achieve Rydberg excitation of an atom, there exist specific requirements that must be met. The simplest atoms for Rydberg excitation are alkali atoms with one valence electron [7]. In this experiment, the alkali atom  $^{87}$ Rb is utilised. It is a non-stable isotope, with a natural abundance of  $(27.83 \pm 0.02)$  % relative to the stable isotope  $^{85}$ Rb [8].  $^{85}$ Rb has a natural abundance of  $(72.17 \pm 0.02)$  % [9]. The non-stable isotope has been shown to exhibit a number of advantages over the corresponding stable isotope  $^{85}$ Rb with regard to evaporative cooling and the more straightforward level structure [8]. It is evident that the rate of decay is also very slow, which serves to further enhance its advantages [9]. Due to the level structure, it is possible to utilise a 780 nm diode laser for the  $D_2$ -line transition into the intermediate state, followed by a second 480 nm diode laser for excitation into the final Rydberg state. This excitation process can be treated as a 2-photon excitation.

Firstly, the definition of Rydberg atoms will be discussed in Section 2.1, followed by an overview of the necessary requirements in Section 2.2.

#### 2.1 Rydberg-states

Rydberg states are the excitation of a valence electron to a high principal quantum number n, which is usually at the order of 10 to 100 in similar experiments [2]. It is therefore possible to treat the Rydberg state as a hydrogen-like atom. In order to solve the Schrödinger-equation of hydrogen, it is possible to use spherical coordinates and divide the equation into radial and angular components. The following describtion is taken from [10] and [6]. In this instance, the radial solutions are found to be regular f and irregular f Coulomb-functions. The following discussion will now address the cases of f = 0 and f = f . In the first case the function is as follows:

$$f(l, E, r) \propto r^{l+1}$$
  
 $g(l, E, r) \propto r^{-l}$ .

For  $r = \infty$  it leads to the hydrogenic Bohr formula

$$E = -\frac{1}{2n^2} \,. \tag{2.1}$$

It is assumed that the valence electron's potential is deeper than -1/r if the distance r to the nucleus is less than the radius  $r_c$  and equal to -1/r for  $r > r_c$ . For  $r < r_c$  the radial part of the Schrödinger-function is different and causes an energy shift, which is called the quantum defect  $\delta_l$ . The new energies are written as

$$E' = -\frac{1}{2(n - \delta_I)^2} = \frac{1}{2n'^2},$$
(2.2)

where n' is the effective quantum number. It was also observed that this energy shift occurs for  $r > r_c$  as well and is caused by core polarisation due to dipol polarisability of the atom's core [6].

The hyperfine splitting plays an important role for the  $D_2$  line transition to the intermediate state  $5P_{3/2}$ . The fine structure describes the coupling between the spin angular momentum S and the orbital angular momentum L and sums up to the total angular momentum L of the electron. Regarding fine structure's selection rules taken from [8] the eigenstates are determined via

$$|L - S| \ge J \ge L + S. \tag{2.3}$$

Thereafter, the ground state of rubidium is characterised by  $5S_{1/2}$  and the intermediate state by  $5P_{3/2}$ . Due to the hyperfine structure there is a further splitting of energy levels. Now the nuclear spin affects the level structure, so the total angluar J and spin momentum I sum up to the total atom's momentum F. The selection rules for the hyperfine structure are equivalent to those of the fine structure. It follows that the ground state has now two additional F-states of F=1 and F=2 with I=3/2 and J=1/2, seen in Fig. 2.1. For the intermediate state the resulting F-states are F=0, F=1, F=2 and F=3 that are visualised in Fig. 2.1. The transition from  $5S_{1/2}$  to  $5P_{3/2}$  is called the  $D_2$ -line transition and is driven at a wavelength of  $(780.241209686 \pm 0.000000013)$  nm [8]. In the experiment, it is excited by the probe laser at 780 nm with a certain detuning  $\delta$ . For the Rydberg transiton a second laser is needed that excites the valence electron to a high n quantum number. This is achieved with the Rydberg control laser at a wavelength of 480 nm and visualised in Fig. 2.1. Additionally, the requirements for the Rydberg excitation are depicted in the following section.

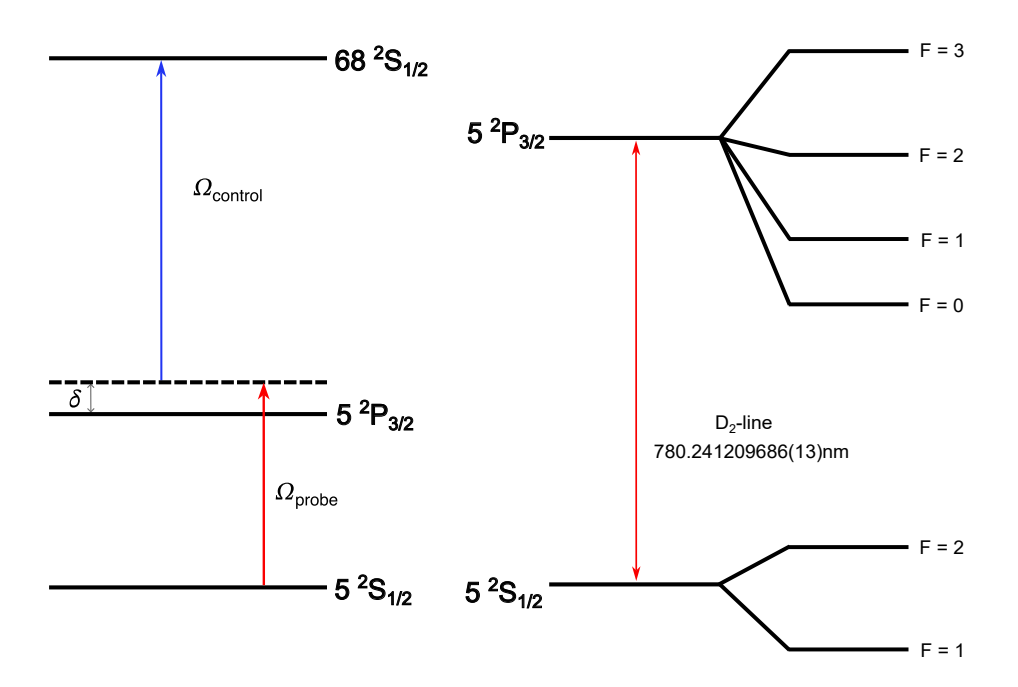


Figure 2.1: The transition based on [11] from the 5 S-state to the 5 P-state of  $^{87}$ Rb is driven by the probe beam is shown in the left picture. The off-resonant excitation to the Rydberg state 68 S is done by the control beam. The hyperfine splitting depends on the polarisation of the probe and control beam and is visualised in the right figure. The hyperfine splitting based on [8] of the  $D_2$ -line transition causes additional F-states for the intermediate and ground state. Now the ground state has two extra F=1 and F=2 states, while the intermediate state has four additional states: F=0, F=1, F=2 and F=3. The transitions between the hyperfine states form a closed cooling cycle that is necessary for the cooling process of the magneto optical trap, which will be discussed later.

#### 2.2 Requirements for Rydberg excitation

In the following, the required conditions for Rydberg excitation of rubidium atoms will be illustrated.

- 1. Trapping and cooling the rubidium atoms, so that they form an atom cloud.
- 2. The wavelength and the detuning of probe and control must be set correctly.
- 3. The overlap of probe, control and the atomic cloud must be optimal at the position the later experiment should be conducted.
- 4. Polarisation of probe and control must be set correctly.

The trapping and cooling processes are already set up and fully characterised by Valerie Mauth in her Bachelor's thesis [12]. In this experiment there are two control lasers that drive the same Rydberg transition. The first Rydberg control laser is already set up and optimised by Samuel Germer in his Bachelor's thesis [13]. This first setup was taken as reference for the setup of the second Rydberg control laser. Based on this, the parameters for the wavelength  $\lambda$  and the detuning  $\delta$  were adopted. The overlap between the probe and the second control beam was established by overlapping the first and second Rydberg control lasers. Later it

was further optimised by adjusting the control beam to ion counts, which is discussed in Section 4.2.2. At last the polarisation of the Rydberg control beam was optimised by maximising the ion count rate. Further explanation can be found in Section 3.3.

### Setup of Rydberg control laser

In this experiment, the Rydberg control laser TASHGpro is a frequency-doubled diode laser from the company TOPTICA PHOTONICS. A diode laser is a type of semiconductor laser based on laser diodes. They work similarly to regular photodiodes, but above lasing threshold. After the recombination of electrons and holes light is emitted via spontaneous emission [14]. The TASHGpro laser unit consists of a frequency stabilised seed laser at 960 nm that is locked to an external cavity according to the PDH method [15]. This method is briefly depicted in Section A.1. This was achieved by Aylin Cansiz in her Bachelor's thesis [16]. The Rydberg control laser at 480 nm is produced using Second Harmonic Generation (SHG) cavity inside the laser box [17].

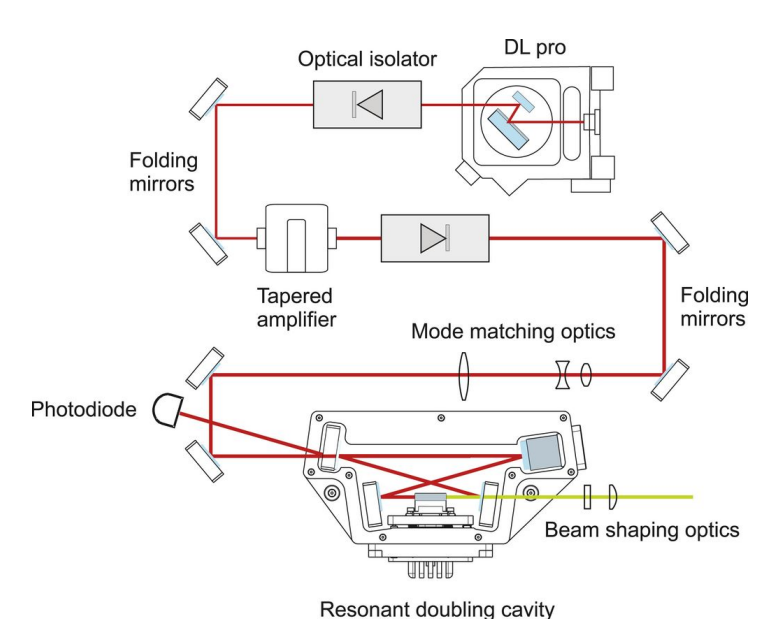


Figure 3.1: The illustration of the TASHGpro laser unit is taken from [18]. It shows the generation of the second harmonic 480 nm wave of the fundamental 960 nm wave. The fundamental beam is produced in the DL pro part of the laser unit. Then it is amplified with the tapered amplifier, and soon it passes optics that leads to mode matching. After this the beam enters the internal cavity where SHG at a nonlinear crystal takes place. Now there are two laser beams, one with doubled frequency, propagating into the same direction. The intensities of the beams depend on each other.

This works as follows: The laser beam of the seed laser passes a nonlinear crystal and induces the generation of a second wave with a nonlinear polarisation that oscillates at double the frequency of the input wave. According to the principle of mode matching, both beams propagate into the same direction [19]. The internal cavity is controlled by the laser's computer software and can auto-align the cavity lock by pressing one button [17]. The internal setup of the TASHGpro laser unit is illustrated in Fig. 3.1. In the following I will describe the optical setup that is necessary to transport the light to the region where the Rydberg excitation should be conducted. This includes optics for beam shaping, optical switches in Section 3.1, mechanical shutters in Section 3.2 and optical fibres in Section 3.3.

#### 3.1 Acoustic optical modulator setup

In this section, the integration and the function of an acoustic optical modulator will be discussed. It is used as an optical switch and power control for the intensity of the Rydberg control laser. In Fig. 3.2 the optical setup for the second Rydberg control is visualised. The first optical part is the  $\lambda/2$  wave plate (hwp). A hwp consists of birefringent materials, which cause different refractive indeces for polarised light in the material [20]. This follows a retardation of light polarised along the slow axis of the wave plate. For a hwp the phase shift between the slow and the fast axis amounts to  $\pi$  [20]. Then follows a Polarised Beam Splitter (PBS) cube. The working principle of a PBS is that the reflected and transmitted beams depend on the polarisation of the incoming beam. The used PBS is from the company Thorlabs and reflects the s-polarised and transmits the p-polarised beam because of a special coating and a cement layer [21]. The combination of a hwp and PBS makes it possible to vary the beam power in the reflected and transmitted arm of the PBS. This is the case because p-polarised light is transmitted while the s-polarised light is reflected and the ratio can be set depending on the setting of the hwp. After this, the optical setup for matching the beam size of the beam that exits the laser unit to the beam size that is needed for the AOM is shown and will be further exemplified in Section 3.1.2.

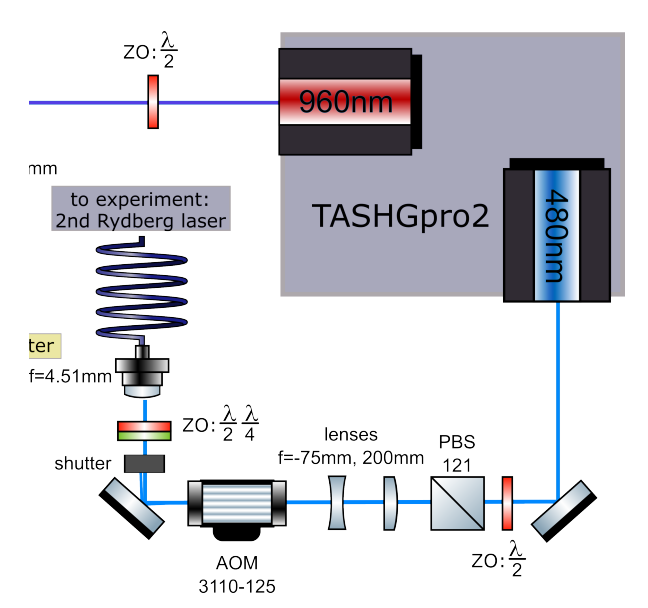


Figure 3.2: The figure shows the laser setup for the Rydberg control laser schematically. The laser beam at 480 nm passes the  $\lambda/2$  wave plate (hwp) and the polarised beamsplitter (PBS), which regulate the power of the incoming beam due to the orientation of the hwp. Then the polarised beam passes a telescope, before the acousto-optical modulator (AOM). The AOM shifts the frequency by  $-110\,\text{MHz}$  into the first order and usually works as intensity control for the experiment. The mechanical shutter blocks the transmitted order which is coupled into a fibre to transport the beam to the experiment chamber. Between fibre and shutter there are two wave plates: a second hwp and a  $\lambda/4$  wave plate. In combination, they adjust the polarisation of the beam before the fibre coupling.

In the following the working principle of the AOM will be discussed. An AOM contains a transparent crystal with a piezoelectric transducer attached to it. This excites a RF wave coming from the RF driver at a frequency of 110 MHz. Due to that a strain wave travels through the crystal. Because of the photo-elastic effect it results in a lattice where the refractive index differs and light experiences Brage diffraction [22]. The diffraction

angle can be calculated via

$$\Theta_{\text{Bragg}} = \frac{\lambda f}{2\nu},\tag{3.1}$$

where  $\lambda$  is the wavelength, f the lights frequency and v the acoustic velocity that depends on the medium [23]. In this setup the light is diffracted into the -1st order to be equivalent with the AOM setup for the first Rydberg control laser. The function of the AOM is to control the transmitted beam power with the RF signal. This driver signal is produced by the AOM driver box that is controlled by the computer control. According to [23] one does reach a maximal AOM coupling efficiency of 85%. These limitations are made by scattering within the crystal. For the used AOM of the company G&H the final maximal efficiency was about 88%. AOMs of G&H can have higher coupling efficiencies [24].

#### 3.1.1 AOM driver box

The RF signal for the AOM is provided by the AOM driver box. It is a frequency generator with high power amplifiers for switching and amplifying the external signal. One box has 4 channels available. Each channel has a digital and a manual input. With a switch one can choose the used input source. This input source originates of a signal generator that is controlled with the computer control. For the high amplified output of the AOM box it is important that one never powers the box without a  $50\Omega$  load which would destroy the high amplifier. In the following it is necessary to program the AOM box for the correct voltage supply of the AOM. The actual output power of the box is about 1 W but the used AOM's saturation power is already 0.39 W for a wavelength of 488 nm [24]. Therefore, an additional attenuator of -3 dB is required for this channel in the AOM box. After this the output voltage can be adjusted with the computer program AD9958\_59 Evaluation. In this program one varies the parameters and specifies the output voltage on the oscilloscope until the corresponding voltage of 0.39 W for this AOM is found.

#### 3.1.2 Telescope

The laser beam that comes out of the laser has the form of a Gaussian beam, but the diameter of the beam is unknown. As it is important to match the beam diameter to the active aparture of the AOM, one has to know the size and adjust accordingly. The radius w of this kind of beam results in dependence of the position z in

$$w(z) = w_0 \sqrt{1 + \left(\frac{z}{z_R}\right)^2},$$
 (3.2)

with beam waist  $w_0$  and Rayleigh length  $z_R$  [25]. Making optimal use of the AOM the laser beam should be collimated. This can be done with a lens system of one convex and one concave lens. With help of the open source software of Gaussian Beam one could construct the lens system and estimate the distances between both lenses that are required for a collimated beam.

#### Beam waist measurement

Before constructing the lens system it is also necessary to know the beam waist of the laser which was unfortunately not specified by the company. The active area of the AOM's crystal is limited to 1 mm, so the beam waist should not exceed it. This leads to the beam waist measurement which was done with the *knife-edge* method [26]. A knife edge is slowly moved into the beam and the beam power is measured in dependence of the position of the edge. For the evaluation, the power with relation to the knife's position is

plotted. This is shown in Fig. 3.3. The function

$$P(z) = \frac{P_0}{2} \left( 1 - \operatorname{erf}\left(\frac{z - z_0}{w / \sqrt{\pi}}\right) \right)$$
 (3.3)

describes the beam power at the position z with input beam power  $P_0$ , distance of the beam center  $z_0$  and  $1/e^2$ -beam radius w and is fitted to the data points in Fig. 3.3 [27].

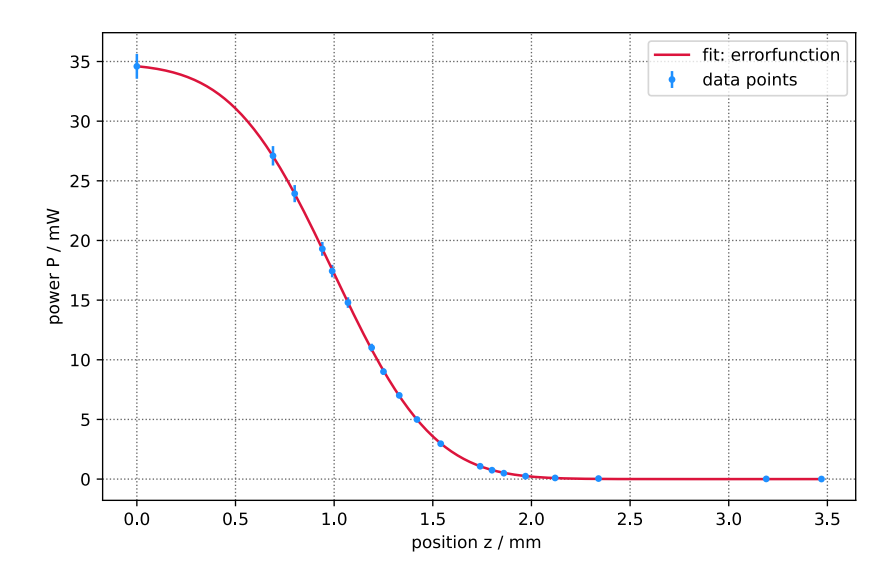


Figure 3.3: This plot shows the beam power P in dependence of the position z of the knife-edge that is moved perpendicular to the beam. The data points are plotted and the function of Eq. (3.3) is fitted to the data points. According to the fit the resulting fit-paramters are:  $P_0 = (34.00 \pm 0.06) \text{ mW}, z_0 = (0.99 \pm 0.01) \text{ mm}, w = (0.80 \pm 0.01) \text{ mm}.$ 

The resulting fit was done with the scipy.optimize package curve—fit and the fit parameters result in

$$P_0 = (34.00 \pm 0.06) \text{ mW}, \quad z_0 = (0.99 \pm 0.01) \text{ mm}, \quad w = (0.80 \pm 0.01) \text{ mm}.$$

With the calculated beam waist w one can construct the final lens system that consists of a convex lens with a focal length of 200 mm and a concave lens with focal length of -75 mm. The resulting beam waist after the convex lens is about 0.3 mm, which is compliant with the maximal beam waist of the AOM.

#### 3.1.3 AOM response curve

For including the intensity control of the beam to the computer sequence, it requires a calibration of the AOM's voltage because of the nonlinear intensity of the beam in RF power. This is achieved with an AOM response curve measurement. To measure it, a photodiode is positioned after the AOM in the diffracted beam while the 0th order is blocked. Then, the connection between signal generator and oscilloscope (red signal in Fig. 3.4), as a reference, and between the signal generator and the manual input of the AOM box (blue signal in Fig. 3.4) is established. The generated signal is a triangular signal with a frequency of 0.5 Hz, an amplitude of  $10 \, \text{V}_{pp}$  and an offset of 5 V. Next, the beam power needs to be regulated so that the power is maximal but does not saturate the photodiode. The resulting signals of the oscilloscope are shown in Fig. 3.4. To calibrate the signal of the AOM, the voltage of the PD is normalised at  $10 \, \text{V}$ . This corresponds to the

maximal voltage that is applied to the AOM driver box. The normalised voltage is plotted inverted against the reference voltage from the signal generator and a polynomial function of the 9th degree is fitted to the data points. The inversion of the signal is done for the compensation of the nonlinearity of the beam's intensity in RF power and for finding a control voltage as a function of the power after the AOM. The resulting plot is visualised in Fig. 3.5.

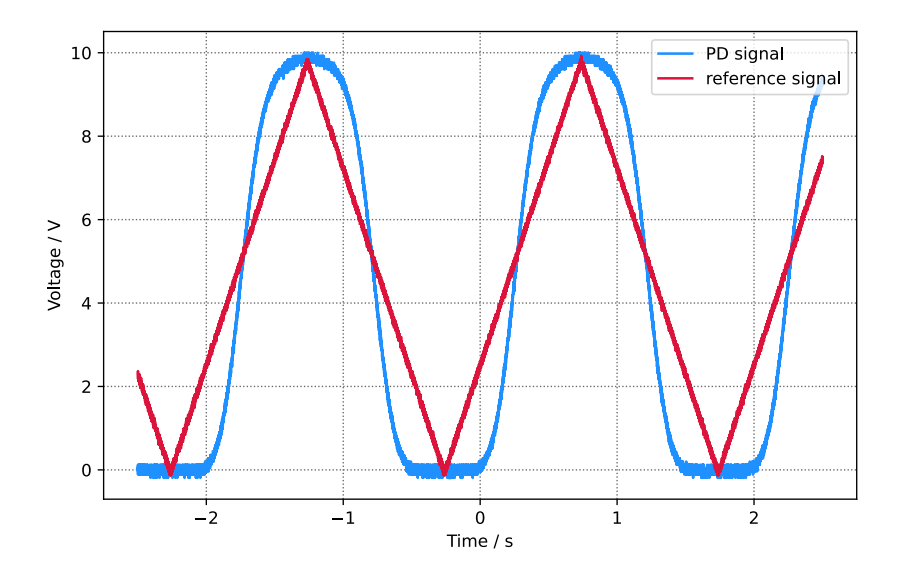


Figure 3.4: The red signal is the triangular reference signal from the signal generator with a frequency of  $0.5\,\mathrm{Hz}$ , an amplitude of  $10\,\mathrm{V}_{pp}$  and an offset of  $5\,\mathrm{V}$ . The same signal is also applied to the AOM. The blue signal is the resulting signal of the photodiode which is positioned after the AOM and measures the voltage of the diffracted order.

#### 3.2 Mechanical shutter

It is essential to ensure that no light of the Rydberg laser enters the experimental chamber when the AOM is switched off. Despite being deactivated, a degree of diffracted light is emitted from the fundamental beam. In order to prevent such occurrences, the implementation of mechanical shutters is necessary. The mechanical shutter used in this experiment consists of a small metallic flag that is mounted on a solenoid from Takano. A mechanical shutter blocks the diffracted beam when it is closed. The mechanism is controlled electronically, with the control sequence being initiated on the computer. It must be emphasised that for these control sequences to function optimally, the shutter's switching mechanism must operate with precision and in a timely manner. It is possible to set acceleration and deacceleration times for the shutter motor. This allows for fine-adjustment to one side guarantee that the shutter is weak enough to not have an impact on laser locks but on the other hand is still strong enough to have a sufficiently fast rise and fall time. Therefore, it is necessary to measure the delay time and the fall and rise times of the recently constructed shutter relative to the applied signal. The delay time between the reference signal and the measured shutter signal is shown in Fig. 3.6.

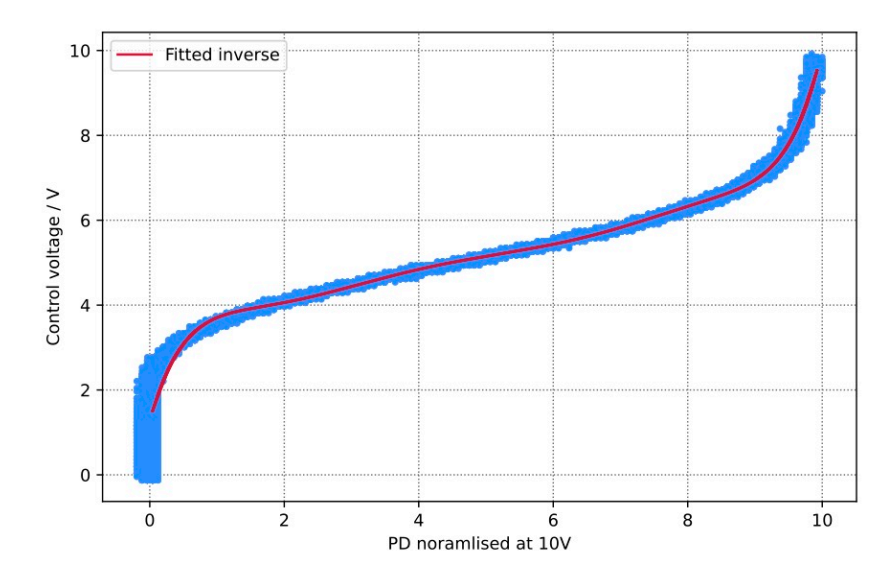


Figure 3.5: The signal produced by the signal generator has a triangular form with a frequency of  $0.5\,\mathrm{Hz}$ , an amplitude of  $10\,\mathrm{V_{pp}}$  and an offset of  $5\,\mathrm{V}$ . This RF signal is applied to an oscilloscope and to the AOM that causes diffraction orders of the transmitted beam. The diffracted beam results in a corresponding voltage of the photodiode (PD) that is positioned in the diffracted beam. The PD voltage is normalised at  $10\,\mathrm{V}$ . The voltage of the PD and the reference voltage are plotted inverted and a polynomial of 9th degree is fitted to the data.

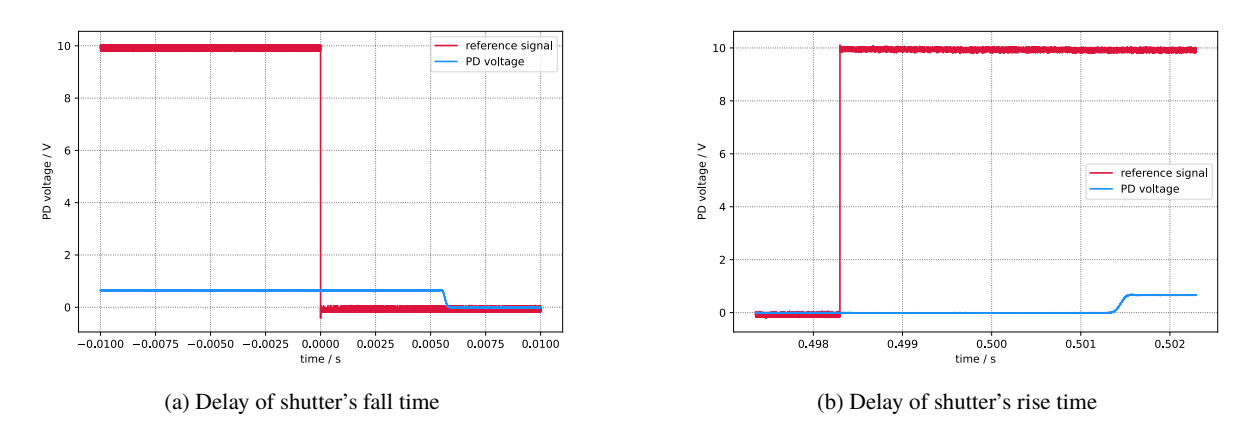
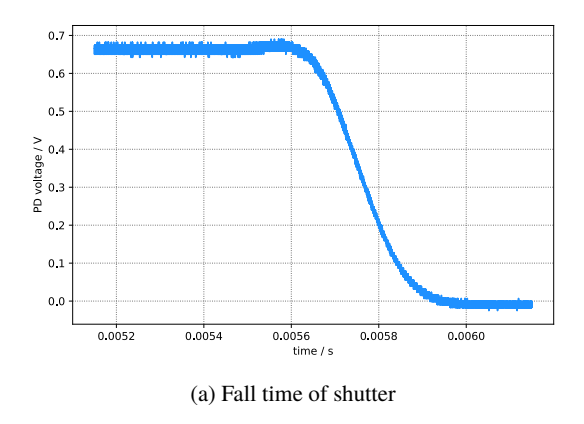


Figure 3.6: The delay time between the shutter signal and the reference signal is determined by the integration of a photodiode. The blue signal is derived from the photodiode, whereas the red signal is designated as the reference signal of the signal generator. In Fig. 3.6(a) the delay time for the closing process is visualised while the reverse process is shown in Fig. 3.6(b). It is possible to estimate the delay times qualitatively from these measurements to  $\tau_{\text{delay fall time}} = 5.7 \, \text{ms}$  and  $\tau_{\text{delay rise time}} = 3.2 \, \text{ms}$ .

According to Fig. 3.6 the delay times for the rise and fall time can be determined qualitatively to  $\tau_{\text{delay fall time}} = 5.7 \, \text{ms}$  and  $\tau_{\text{delay rise time}} = 3.2 \, \text{ms}$ . The delay times are important to know as they have to be accounted for in the computer control to make sure the shutter opens and closes at the wanted time without any delay. The fall and rise times are determined by the duration required for the shutter complete its to opening and closing cycles. Fig. 3.7(a) shows the closing process of the shutter which has a fall time of  $\tau_{\text{fall time}} = 0.35 \, \text{ms}$ . The corresponding rise time is visualised in Fig. 3.7(b) and amounts to  $\tau_{\text{rise time}} = 0.22 \, \text{ms}$ . Both, fall and

rise time are fast enough for their purpose. As the control laser will be on or off for times much longer than 0.3ms during a Rydberg sequence, the set values are sufficiently fast. This is why the measurement could be conducted qualitatively, and no data fit was required.



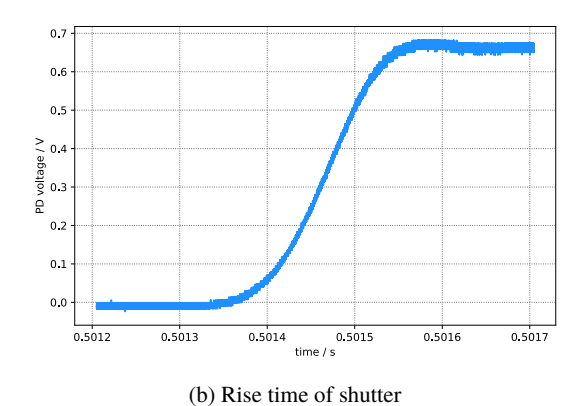


Figure 3.7: In Fig. 3.7(a) and Fig. 3.7(b) the voltage of the photodiode in dependence of the time is visualised. The fall and rise time of the shutter refers as the time the shutter needs for the open and close mechanism. It is determined by the integration of a photodiode. In Fig. 3.7(a) the fall time for the closing process is visualised while the reverse process is shown in Fig. 3.7(b). It is possible to estimate the fall and rise times qualitatively from these measurements to  $\tau_{\text{fall time}} = 0.35 \, \text{ms}$  and  $\tau_{\text{rise time}} = 0.22 \, \text{ms}$ .

#### 3.3 Fibre coupling and polarisation

After the laser light can be controlled by an AOM and optical shutter, it is important to guide the light to the location where the Rydberg excitation should be performed. Therefore, a single mode polarisation maintaining glass fibre is used. A glass fibre has a cylindric shape and consists of a core material that is surrounded by a cladding. The whole fibre is coated by an isolation. The decisive requirement for light guiding through the fibre is that the refractive index of the core  $n_{\text{core}}$  must be larger than the refractive index of the cladding  $n_{\text{cladding}}$  [28]. The successful transmission of laser light into the fibre is dependent upon its angle of incidence, which is essential for the effective guidance of the light into the fibre's core region. Furthermore, it is able to travel through the fibre by totally reflecting from the edges of the core region [28]. The transport of light with optical fibres results in a loss of intensity of the beam's power. The main losses originate from impurity of manufacturing processes, internal scattering or bending [29]. It is evident that, from all the sources of loss, a mere 70% of the actual beam is transmitted for a wavelength of 488 nm [30]. For the optimisation of the fibre coupling, the polarisation of the laser beam must be adjusted properly to fibre's polarisation axis. This is achieved with the half-wave plate and the quarter-wave plate (qwp) that are illustrated in Fig. 3.2. The function of the hwp has already been explained in Section 3.1. The working principle of the qwp is similar. Instead of retarding the slow axis of  $\pi$ , it is retarded by  $\frac{\pi}{2}$  that changes the polarisation of the light [20].

The polarisation of the fibre drifts over time due to thermal and mechanical stress. To measure the drifts of the polarisation, the fibre is connected with a polarisation analyser <sup>1</sup>. Thereafter, the analyser is connected with the computer control and the program SKP PolarizationAnalyzer is started. For this measurement it is important to lower the power of the control beam, otherwise the polarisation analyser is saturated. Then, the

<sup>&</sup>lt;sup>1</sup> of the company Schäfter+Kirchhoff

measurement is conducted by slightly heating the fibre by touching it. The drifting polarisation is visualised in Fig. 3.8, which is optismised afterwards. The final polarisation is set to horizontal, which corresponds to the polarisation of the fibre, and is shown in Fig. 3.9. The Polarisation Exctinction Ratio (PER) describes the relation of power between the principal polarisation mode and the orthogonal polarisation mode after propagating through a medium [31]. After optimisation of the polarisation the mean PER amounts to 47.8 dB and the minimum PER to 43.6 dB. These values are much higher than the company's reference values [30], where the minimum PER is stated as 18 dB. This is due to the short-term measurement that is done with the polarisation analyser, whereas the PER may decrease over a longer period of time.

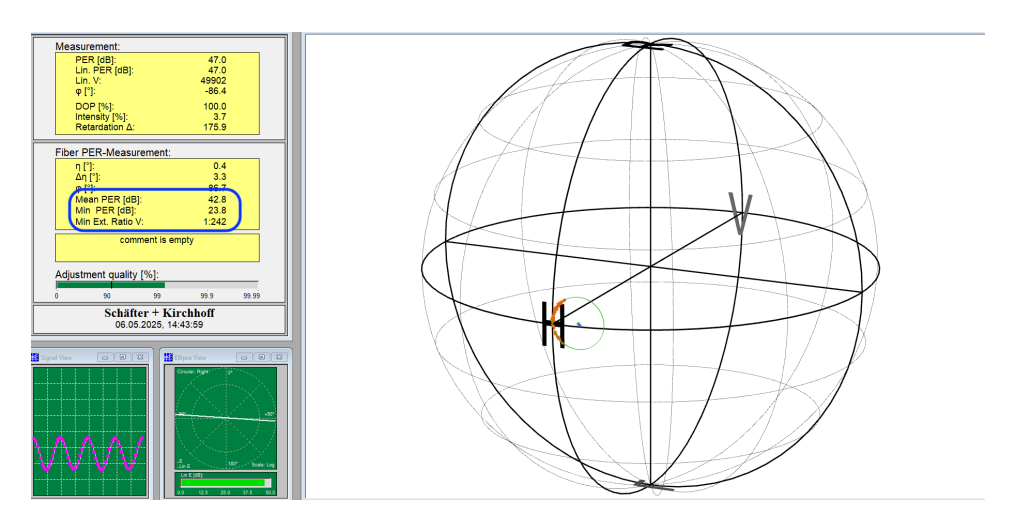


Figure 3.8: The polarisation of the fibre is not stable on long terms. It drifts over time due to thermal and mechanical stress. The measurement of the polarisation drift is shown with the green circle. In the blue box, the mean PER and the minimal PER are visualised before the optimisation.

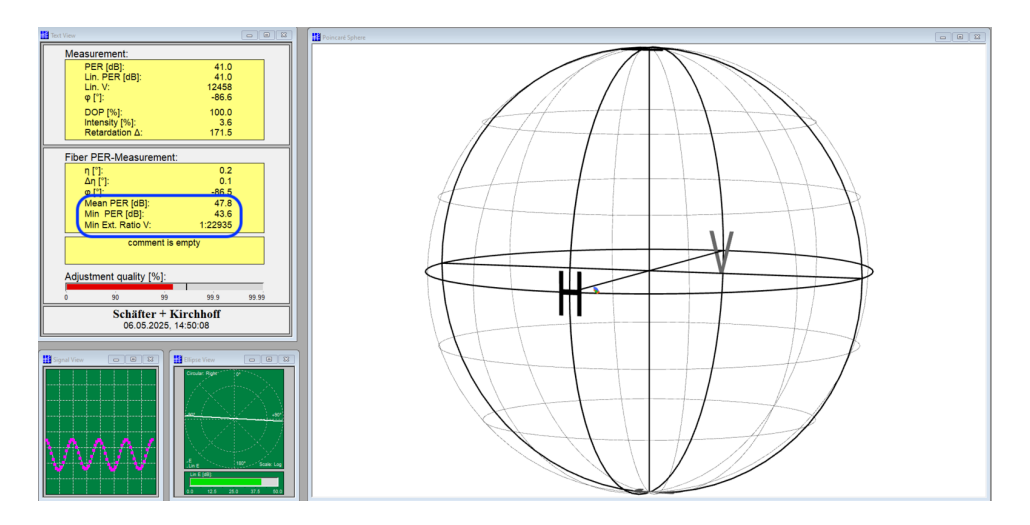


Figure 3.9: The optimisation of the polarisation drifts of the fibre are shown. In the blue box, the mean PER and the minimal PER of the final polarisation adjustment are visualised. The optimisation of the polarisation is achieved with the adjustment of the hwp and the qwp.

### CHAPTER 4

# **Rydberg excitation measurements**

In the previous chapter, the preparation of the control laser for the Rydberg excitation was elaborated. In this context, requirements for Rydberg excitation, the control of the beam power with the AOM and the polarisation of the beam before the fiber were discussed. In this chapter, the process of the Rydberg excitation measurement will be outlined. The first Section 4.1 provides an overview of the preparation of rubidium atoms in a Magneto-Optical Trap (MOT) and the magnetic transport of the atoms to the science chamber. Thereafter, each step in the process of the final Rydberg measurement will be illustrated in the second Section 4.2, starting with the determination of the wavelength and the detuning of the control laser.

#### 4.1 Atom preparation and characterisation

The experimental setup is divided into two sections. The first part of the optical setup on the experiment table contains the MOT, which traps and cools the rubidium atoms. The second part of the setup is the Science Chamber (SC), where the atoms are excited into the Rydberg state. A magnetic transport is used to connect both chambers, which transports the atoms to the SC. In the following, the trapping and cooling process in the MOT chamber and the magnetic transport are briefly described.

The rubidium atoms are trapped by the beam power of three orthogonal laser pairs. The complete cooling process of a MOT can be found in [32]. The trapped atoms are cooled by the TApro 1 laser, which is called cooler, to decrease their temperature via Doppler-cooling. This is achieved by driving the transition from  $5\,S_{1/2}$  to  $5\,P_{3/2}$  red-detuned. The atom itself moves in direction of the laser, which causes the transition to be on resonance, and absorbs the incoming photon. The absorbed photons decay via spontaneous emission in an arbitrary direction back into the ground state  $5\,S_{1/2}$ . Due to the random direction of the resulting emitted photons the total momentum is averaged to zero [32]. Due to rethermalisation via atom collisions in the cloud, the overall temperature is reduced.

To reach temperatures below the Doppler limit, the cooling process of optical molasses can be used. This process is discussed in [33]. This results in the magnet field being deactivated, with the cooling process being primarily executed by the orthogonal laser pairs in each direction. The process of laser cooling by optical molasses in addition with Sisyphus-cooling results in the production of atoms that possess a temperature below the Doppler limit, yet considerably above the recoil limit [32].

After the molasses phase, the state of the atom is not well defined, but only atoms in the F=2  $m_F=(1,2)$  state are trapped by the magnetic trap for the magnetic transport. Therefore, optical pumping is performed on the transition from ground state F=2 to the intermediate state F=2, so that all atoms are pumped into the dark state  $|F=2,m_F=2\rangle$ . It is also possible to decay into lower states from the intermediate state, but these are not part of the pumping cycle. To prevent the loss of atoms there is another laser, the DLpro 2, that works as a repumper. It pumps the atoms back into the  $5S_{1/2}$  with F=1 to  $5P_{3/2}$  F=2 by driving  $\sigma_+$  transitions [34]. Thereafter, the atoms are excited again by the optical pumping laser until all atoms are in the dark state.

After the optical pumping in the MOT chamber, the atom cloud is transferred to a magnetic trap, which is created by the MOT coils such that it can then be magnetically transported to the science chamber. The magnetic trap in the MOT chamber is realised by quickly ramping the coil current that produces a stronger magnetic field gradient trapping the atoms. The transport process can be read in detail in the Master thesis of Valerie Mauth [35]. After the transport the atoms are held in the position by the magnetic trap, where the Rydberg excitations will take place. This magnetic trap is generated by the last coil pair of the transport. To check, whether the transport was successful, the number of atoms in the final trap is measured for different trap holding times using absorption imaging. The holding time corresponds to the time during which the atoms are held in the trap, while the magnetic field is applied. In Fig. 4.1 the atom number and the corresponding holding time in the SC are visualised. An exponential function of the form

$$N(t_{\text{hold}}) = N_0 \left( 1 - \exp \frac{-t_{\text{hold}}}{\tau} \right)$$
 (4.1)

is fitted to these data points, which is taken from [36]. N is the atom number at holding time t,  $N_0$  the initial atom number and  $\tau$  the lifetime of the atoms. According to the data fit of the holding time measurement in the science chamber, the atom number results in  $(2.760 \pm 0.124) \times 10^8$  and their lifetime amounts to  $(10.93 \pm 1.03)$  s. These values agree with usually recorded data of the science chamber [34] and show that

the atom preparation for the Rydberg excitation is working.

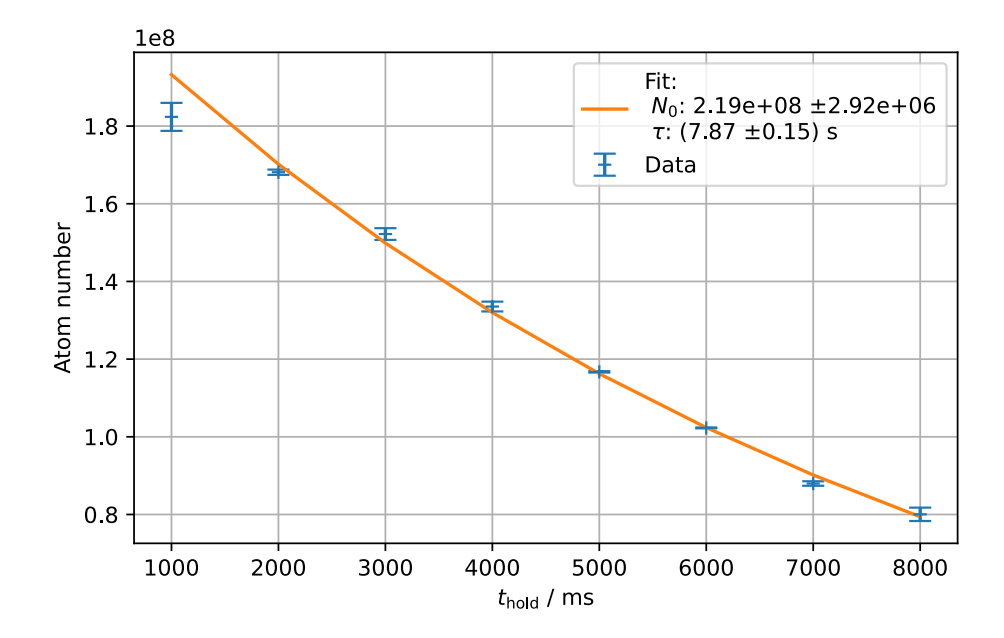


Figure 4.1: The atom number for different holding times in the science chamber. The atom cloud is transferred to the SC using the magnetic transport. There, the atoms are held in place for a variable time. Some atoms are lost due to background collisions from the trap. An exponential function is fitted to the data point, from which the atom number and the lifetime of the atoms can be extracted. Each datapoint is the average of two measurements.

#### 4.2 Rydberg excitation and detection

After the atom preparation, the atoms are in the ground state. Subsequently, the probe beam excites the atoms into the  $5P_{3/2}$ -state. The Rydberg transition is driven from  $5P_{3/2}$  to  $68S_{1/2}$  by the Rydberg control beam at 480 nm. Before this can be done, the wavelength and the detuning of the Rydberg control beam must be adjusted and the alignment between probe and control must be optimised. Both will be explained in Section 4.2.1 and Section 4.2.2.

#### 4.2.1 Detuning of Rydberg control laser

In Fig. 2.1 the transitions of probe and control with a detuning  $\delta$  are illustrated. In the following, the process of the determination of the correct wavelength and the detuning of the Rydberg transition is described. The wavelength and the detuning of the control laser is configured with a RF signal generator  $^1$ . This device modulates sidebands to the original frequency of the seed laser. The seed laser is locked if one sideband overlaps with the transmission frequency of the cavity. It is necessary to mention that Rydberg excitation occurs if the detuning offset of the control is compensated by the detuning of the probe laser. The wavelength of the control laser can be approximately adjusted to align with the target transition by using a wavemeter. In order to execute fine-tuning, it is necessary to utilise the atoms as a reference. For this purpose, the control

<sup>&</sup>lt;sup>1</sup> SynthUSBII - USB RF signal generator from Windfreak technologies

light is guided to the MOT chamber and superimposed with the optical pumping laser beams, such that it hits the MOT centrally, while the MOT is loading. If the combination of wavelength of control and wavelength of probe matches the two-photon resonance to the Rydberg state, it causes the excitation of Rydberg atoms, which are not longer trapped in the MOT. This reduction of fluorescence is visualised in Fig. 4.2. The fluorescence of the atoms in the MOT chamber results of spontaneous emission of the previously excited atoms in the cooling process. Therefore, the wavelength of the control is tuned and simultaneously the fluorescence of the MOT is monitored.

In the following the RF value of the signal generator is set to 559.25 MHz and the wavelength, where the seed laser is locked, amounts to 959.3169 nm.

In Fig. 4.2 a life camera image (blue box) of the monitored MOT fluorescence is shown together with the total MOT fluorescence summed up within a suitable region of interest for the last 1000 images (green box). One can clearly see a strong drop of the fluorescence after image 200 which indicates, that the control was successfully tuned into resonance at that point.

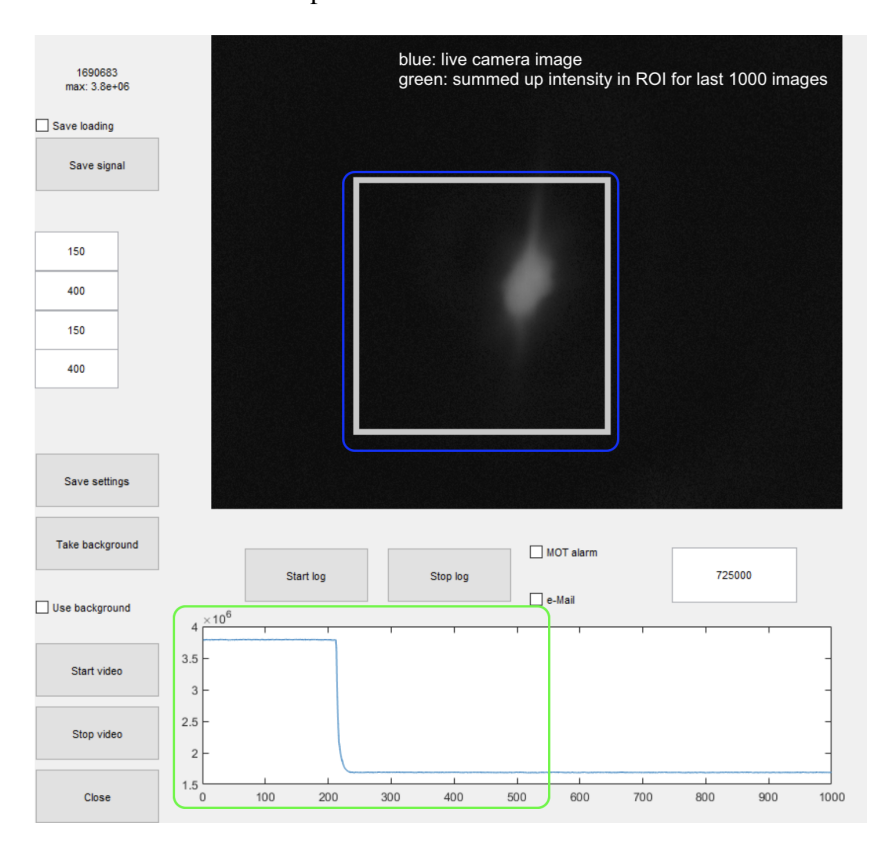


Figure 4.2: The blue box shows the live camera image of the fluorescence in the MOT chamber. The summed up intensity of the fluorescence in the region of interest of the last 1000 images is seen in the green box. This fluorescence is produced by atom in the excited state, which de-excite and emit light. It vanishes if the two-photon resonance is excited and Rydberg atoms are created, which leave the magnetic trap.

#### 4.2.2 Alignment of probe and Rydberg control laser

In the following, the probe-control laser setup of the experimental table, shown in Fig. 4.3, will be described. Since the setup is mirrored, only the optical setup of probe 2 and control 2, which where utilised during the thesis, are discussed in detail.

The probe and the control light are each guided by an optical glass fibre to the experimental table. The probe beam is linearly polarised by the polariser implemented in the outcoupler. Each beam is guided through the combined qwp and hwp. Thereafter, the probe and control beam are superimposed with a dichroic mirror. The achromatic lens between the glass cell and the dichroic mirror is used to focus each beam onto the atom cloud in the SC. After the light is transmitted through the glass cell, it enters the reflected arm of the PBS, where only the probe beam is able to pass, and hits the interference filter of the Single Photon Counter Module (SPCM), thereafter it is detected.

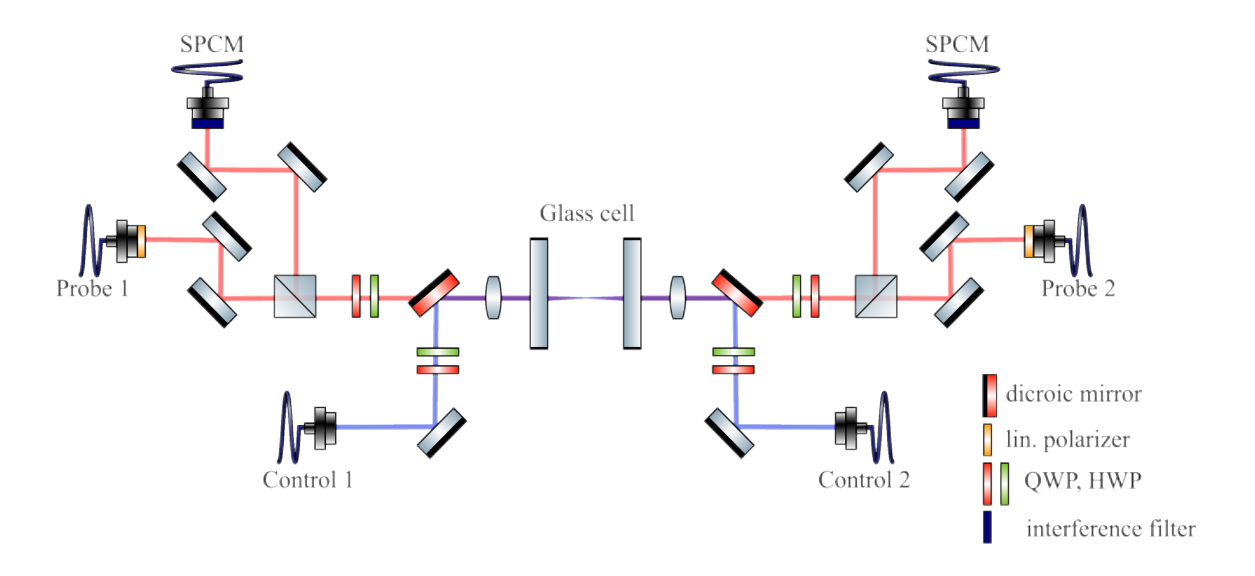


Figure 4.3: The schematic setup of the experimental table is fabricated by Julia Gamper and taken from her Master's thesis [34]. The polarisations of the second Rydberg excitation laser and of the linear polarised probe laser are adjusted. Therefore, the qwp and hwp are adjusted to  $\sigma_+$ -polarisation for the probe beam and to  $\sigma_-$ -polarisation for the control beam. Both beams are superimposed with the dichroic lens and focused into the science chamber with an achromatic lens that follows.

Subsequently, it is required that the Rydberg control beam has the appropriate polarisation for the Rydberg excitation. In Fig. 4.4 the probe and control transitions from Fig. 2.1, modified with the  $m_{\rm F}$ - and  $m_{\rm J}$ -states, are illustrated. The F-states of the Rydberg states cannot be resolved. For these transitions, the polarisations of both the probe and the control beam must be coordinated with each other. The ground state provided from the atom preparation is  $5S_{1/2}$  with F=2 and  $m_{\rm F}=2$  [34]. The probe laser is circular polarised and therefore, it drives the transition  $\sigma_+$  or  $\sigma_-$ . This depends on the direction of the magnetic field at the position of the atoms. Since the atoms are trapped in a quadrupole field, the magnetic field is flipped in the center of the trap. Therefore, one half of the atoms in the cloud drive the  $\sigma_+$ , while the other half drives the  $\sigma_-$  transition. The polarisation of the probe must be exactly opposite to the polarisation of the probe beam, otherwise the atoms of one side are not excited to the Rydberg state or the excitation is suppressed. In Fig. 4.4 the possible

transitions for the correct polarisation alignment in the quadruple trap is visualised. In this experiment the probe beam drives the  $\sigma_+$ -transition to the intermediate state  $5P_{3/2}$  with F=3 and  $m_F=3$ . Thereafter, the intermediate state is excited by the  $\sigma_-$ -polarised control beam to the Rydberg state of  $m_J=\frac{1}{2}$ . In the illustrated level scheme, there are also possible transitions which lead into other states. Only the transitions being used in this experiment are illustrated in Fig. 4.4. This is why the polarisation of the control beam must be adjusted to match that of the probe. Otherwise, non-existent or unintended transitions will be induced.

The alignment of the probe and control beam with the atom cloud is decisive for the Rydberg excitation. The following steps needed to be done to align the control 2. The second control beam is superimposed with the first control beam by eye. This guarantees approximate alignment, since the first control is already correctly aligned. Afterwards, the overlap between the control laser and the atom cloud is continued by optimising to detected ion counts. These ions result of the excited Rydberg atoms that are ionised by a strong electric field. Afterwards, the positively charged ions are accelerated to a detector. This detected number of ions is proportional to the number of Rydberg atoms and can be used to optimise the alignment. This measurement process is explained in more detail in [34]. For further optimisation the first control beam is coupled back into the laser setup of the second control. Thereafter, the alignment was sufficient for Rydberg excitation. It could be observed that a better alignment of probe and control results in more Rydberg atoms.

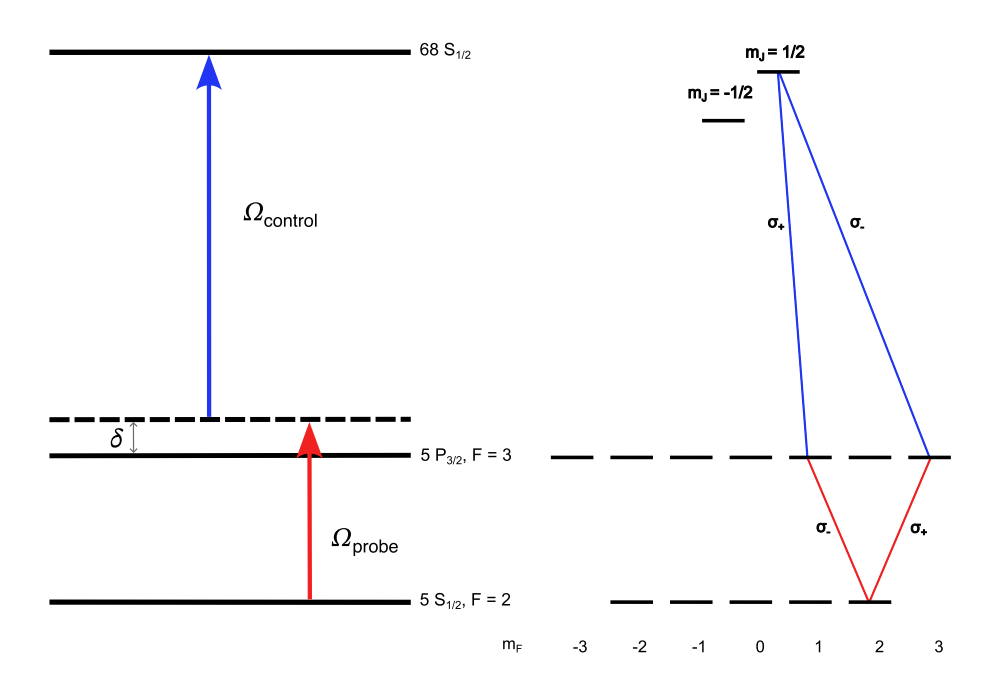


Figure 4.4: The Fig. 2.1 is modified with the hyperfine splitting of the  $m_{\rm F}$ -states based on [34]. The resulting ground state is  $5S_{1/2}$  with F=2 and  $m_{\rm F}=2$ . The probe beam drives the  $\sigma_+$  and ends in  $5P_{3/2}$  with F=3 and  $m_{\rm F}=3$ . The first intermediate state is excited into the Rydberg-states with the transition of  $\sigma_-$ . While the latter state can only be excited with the  $\sigma_-$  transition into the Rydberg state.

The adjustment of the control polarisation is performed using a polarisation analyser of the company Schäfter+Kirchhoff. It is integrated into the experimental setup on the experiment table, so that the beam hits the surface of the polarisation analyser. Before the detection, the beam passes through a qwp and a

hwp, which serve to adjust the beam's final polarisation. The polarisation of the control beam is adjusted with the two wave plates to left-circular light, whereby the resulting Rydberg state is  $68S_{1/2}$ .

#### 4.2.3 Measurement of Rydberg signal in single photon regime

After the previous delineation of the preparation of the atoms, the adjustment of the appropriate wavelength and detuning and the final alignment of the control laser, the following discourse will address the detection of Rydberg atoms. For this measurement Single Photon Counter Modules (SPCM) are used, which allow the detection of Rydberg excitation by detecting single photons. The SPCM detects the spectroscopy signal of the probe light that is transmitted through the atom cloud. Their detection principle is explained in [34] and will just be mentioned shortly. The transmitted probe light is detected by an avalanche photodiode, after which the signal is amplified and the detected photon signal is converted to an electronic signal, which is directed to the computer control. The SPCM's have a very low damage threshold with regard to the count rate, therefore an attenuation of the probe beam is necessary [37]. The probe power is reduced by the implementation of neutral density filters into the laser setup on the laser table.

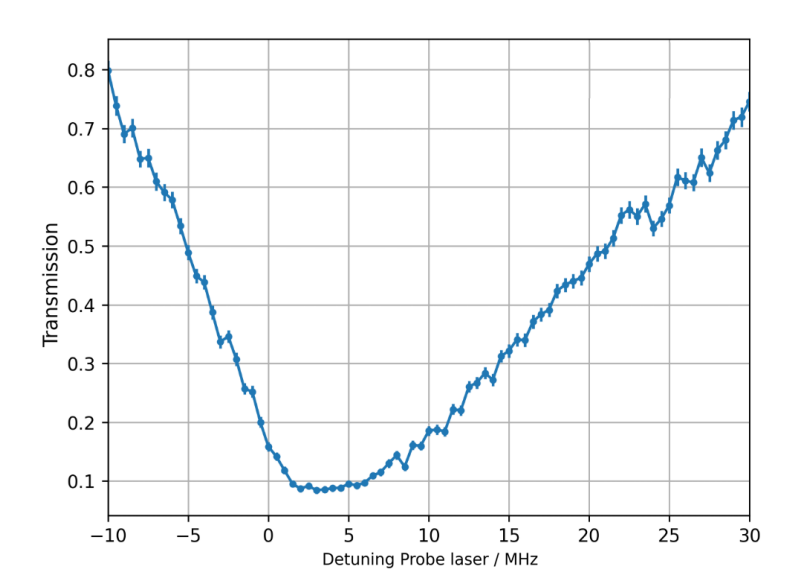


Figure 4.5: The figure shows the transmission of the probe beam through the atom cloud, which is trapped in the quadrupole trap of the science chamber, with the variation of the probe laser's detuning. The data points are averaged over 1000 pulses.

If the Rydberg control light is turned off, the probe light is absorbed by the atom cloud. This is illustrated in Fig. 4.5. It can also be seen from Fig. 4.5 that the optimal absorbtion of the probe beam is not centered around zero detuning, more likely between 0 MHz and 5 MHz, which follows from a slight miscalibration of the x-axis. The absorption spectrum is expected to be a Doppler-broadened Lorentz-curve with a line width that corresponds to the line width of the  $5P_{3/2}$ -transition [32]. In Fig. 4.5 the transmission curve has an asymmetric shape, which results from the quadruple trap, where the quantisation axis of the atom cloud is swapped.

The successful excitation of Rydberg atoms can be confirmed by measuring one of its characteristic signatures

[38]. Therefore, electromagnetically induced transparency is measured. This is shown in Fig. 4.6. This phenomenon occurs if the probe and control lasers are on resonance for the transitions  $5S_{1/2}$  to  $5P_{3/2}$  and  $5P_{3/2}$  to  $68S_{1/2}$ . In the following, the principle of eit in the dressed state picture is shortly explained, according to [38]. The control beam couples between the intermediate  $5P_{3/2}$  and the Rydberg state  $68S_{1/2}$ . This causes a splitting of the intermediate state to the dressed states  $|+\rangle$  and  $|-\rangle$ . The reduced absorption of the probe light, which can be observed in Fig. 4.6, can be explained by the destructive interference between the transitions of ground to the dressed states  $|+\rangle$  and  $|-\rangle$  [38].

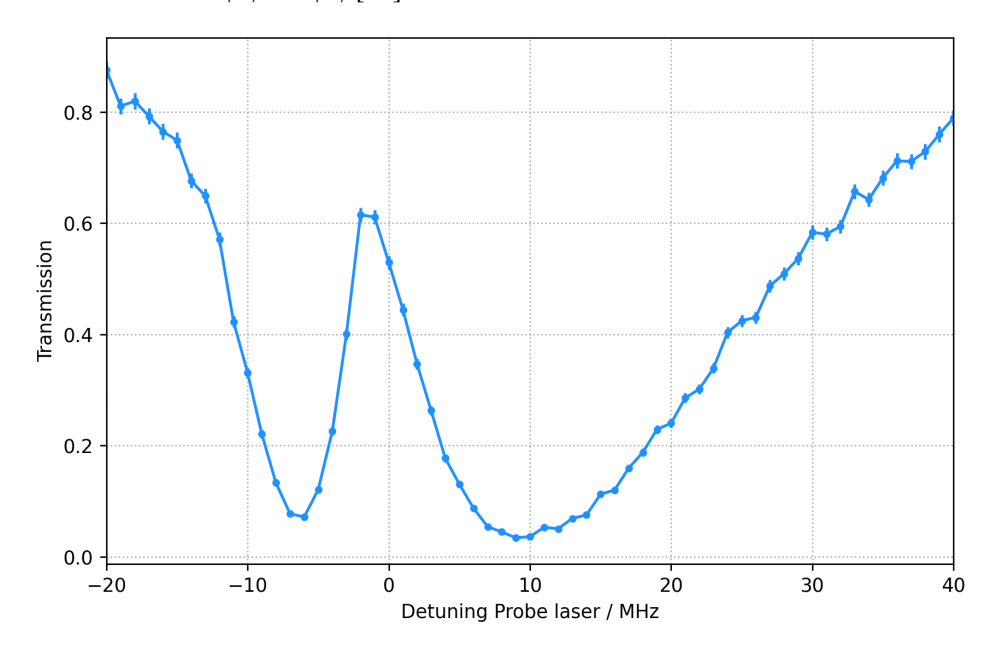


Figure 4.6: The figure shows the transmission of the probe and control beam through the atom cloud, which is trapped in the quadrupole trap of the science chamber, with the variation of the probe laser's detuning. The electromagnetically induced transparency is visible around the zero detuning in the OD valley. Each data point is averaged over 1000 pulses.

### **Conclusion and Outlook**

This thesis, contains the implementation of the second Rydberg control laser for Rydberg excitation of <sup>87</sup>Rb to the setup of the hybrid quantum optics experiment.

In Chapter 2 Rydberg states were introduced and explained. In this experiment, the alkali isotope Rubidium-87 is used as a source and excited to a state with a high principle quantum number n. For the creation of Rydberg atoms, two different lasers are needed to drive the transition to the intermediate state and then to the Rydberg state. The first transition is achieved by the probe beam that drives the  $D_2$ -line transition from  $5S_{1/2}$  to  $5P_{3/2}$ . The Rydberg control laser excites the atom from the intermediate state  $5P_{3/2}$  to the final Rydberg state. In combination, the probe and control laser are able to excite a wide range of Rydberg states. In this work, the control laser is tuned to excite the  $68S_{1/2}$ -state for which the first generation atom chip of the experiment is designed [39]. Before the final excitation takes place, there are requirements that must be met: The atoms are trapped and cooled, which is done in the magneto optical trap. Then, the wavelength of the control laser and its detuning relative to the Rydberg transition are adjusted and the alignment between probe, control and atom cloud is optimised. At last, the polarisation of the control and probe beam are coordinated to each other. Chapter 3 first delineates the optical setup before the fibre and then discusses the transport of the control light via glass fibre. In the first part, the optical configuration for the Rydberg control laser is described, with a particular emphasis on its individual components. One such component is the acousto-optic modulator (AOM), which fulfils dual functions as both a means of power control and as an optical switch within the setup. In order to facilitate its implementation within the computer-controlled system, the AOM's response curve was characterised through experimental means. It shifts the frequency of the control light depending on the coupled order. For the second control beam, the light is coupled into the -1st order, which shifts the beam of -110 MHz. The corresponding AOM voltage is applied by the AOM driver box, which is programmed by the computer control. In order to ensure optimal performance, it is essential that the input beam is collimated and has a suitable waist size. It is also important to note that the diffraction efficiency and the switching speed of the AOM depend on the beam diameter. The beam was resized using a telescope to achieve a waist that would allow efficient diffraction and short switching times. The beam waist of the laser was estimated with a beam waist measurement using the knife-edge method. With the results of the measurement, an appropriate telescope was implemented. Since the AOM still transmits a small proportion into the first order at high power, a mechanical shutter that blocks the transmitted beam was included to prevent unwanted light in the experiment. Therefore, a perfect timing of the shutters is crucial. So, the fall and rise times of the shutter and its delay are measured. These resulting times are less than the switching times of the control laser. In addition, the delay times could have been included into the computer control sequence.

The second part contains the transport of the control light to the experiment, which is done with a single mode polarisation maintaining glass fibre. In order to guarantee the stability of the polarisation, which is fundamental for the accurate alignment of the atomic level, the polarisation of the light is matched with that of the fibre.

The last Chapter 4 provides an overview of the preparation of rubidium atoms in the MOT chamber and the detection of Rydberg excitation in the science chamber. In order to estimate the atom number and temperature, a characterisation measurement is performed within the MOT chamber. This process is essential to ensure correct atom preparation. The same measurement is performed in the science chamber after the magnetic transport. For the Rydberg excitation the wavelength and the detuning of the control laser are adjusted. This is determined with the vanishing of fluorescence when the control beam is guided into the MOT chamber. Thereafter, the alignment between the second control laser and the existing probe and control lasers is modified to achieve optimal overlap with the atom cloud. This was achieved by indirectly measuring an increase in the number of excited Rydberg atoms, as indicated by the detected ion signal. At last, the polarisation of the control beam is adjusted to left-circular, which is coordinated with the polarisation of the probe beam, which is right-circular, to ensure Rydberg excitation. The Rydberg excitation of the rubidium atoms can be observed as an EIT peak in the center of the absorption dip of the probe light.

In the future, the Rydberg control setup can be expanded by adding a fast intensity lock. This intensity lock compensates drifts over time due to decreasing output power of the laser and varying diffraction efficiency of the AOM or of degrading fibre coupling and changes in polarisation. It can be achieved by stabilising the output intensity with a feedback loop.

### APPENDIX A

### **Appendix**

#### A.1 Pound-Drever-Hall Method

In the following the Pound-Drever-Hall method is briefly explained [15]. It is a method to measure the phase of a laser signal indirectly. Thereafter, an error signal is produced, which couples back to the initial laser signal. The method works as follows. The laser is locked to a stable frequency reference. In this experiment, the reference is an ultra-low-expansion cavity. This cavity must fulfill the requirements of a small frequency line width and has to be stable for all timescales. The laser is stabilised to its resonance. The frequency drifts shall be compensated, therefore the error signal is coupled back to the laser signal. When looking at the transmission signal, the visible drifts can originate from frequency drifts or intensity fluctuations. In addion, the drifting direction cannot be estimated. Thereafter, it makes sense to observe the reflected signal because it is zero if the laser is stabilised to a resonance of the cavity. The direction of the drifts can be determined by measuring the phase of the reflected signal, which is antisymmetric around the resonance frequency.

### **Bibliography**

[1] J. P. Dowling and G. J. Milburn, *Quantum technology: the second quantum revolution*, Philosophical Transactions of the Royal Society of London. Series A: Mathematical, Physical and Engineering Sciences **361** (2003) 1655,

```
URL: https://doi.org/10.1098/rsta.2003.1227 (cit. on p. 1).
```

- [2] O. Firstenberg, C. S. Adams and S. Hofferberth,

  Nonlinear quantum optics mediated by Rydberg interactions,

  Journal of Physics B: Atomic, Molecular and Optical Physics 49 (2016) 152003,

  URL: https://dx.doi.org/10.1088/0953-4075/49/15/152003
  (cit. on pp. 1, 3).
- [3] J. M. Gambetta, J. M. Chow and M. Steffen,

  Building logical qubits in a superconducting quantum computing system,

  npj Quantum Information 3 (2017) 2, ISSN: 2056-6387,

  URL: https://doi.org/10.1038/s41534-016-0004-0 (cit. on p. 1).
- [4] M. Saffman, T. G. Walker and K. Mølmer, *Quantum information with Rydberg atoms*, Reviews of Modern Physics **82** (2010) 2313, ISSN: 1539-0756, URL: http://dx.doi.org/10.1103/RevModPhys.82.2313 (cit. on p. 1).
- [5] G. Kurizki et al., Quantum technologies with hybrid systems,
  Proceedings of the National Academy of Sciences 112 (2015) 3866, ISSN: 1091-6490,
  URL: http://dx.doi.org/10.1073/pnas.1419326112 (cit. on p. 1).
- [6] T. F. Gallagher, "Rydberg Atoms", Springer Handbook of Atomic, Molecular, and Optical Physics, ed. by G. W. F. Drake, Cham: Springer International Publishing, 2023 231, ISBN: 978-3-030-73893-8, URL: https://doi.org/10.1007/978-3-030-73893-8\_15 (cit. on pp. 1, 3).
- [7] "Nichtlineare Spektroskopie", *Laserspektroskopie: Grundlagen und Techniken*, Berlin, Heidelberg: Springer Berlin Heidelberg, 2007 299, ISBN: 978-3-540-33793-5, URL: https://doi.org/10.1007/978-3-540-33793-5\_7 (cit. on p. 2).
- [8] Rubidium 87 D Line Data,
  URL: https://steck.us/alkalidata/rubidium87numbers.1.6.pdf (visited on 03/07/2025) (cit. on pp. 2-4).
- [9] Rubidium 85 D Line Data,
  URL: https://steck.us/alkalidata/rubidium85numbers.pdf (visited on 03/07/2025) (cit. on p. 2).

- [10] G. Drake, *Springer Handbook of Atomic, Molecular, and Optical Physics*, 2006, ISBN: 978-0-387-20802-2 (cit. on p. 3).
- [11] A. Banerjee, D. Das and V. Natarajan,

  Precise fine-structure and hyperfine-structure measurements in Rb, 2002,

  arXiv: physics/0209019 [physics.atom-ph],

  URL: https://arxiv.org/abs/physics/0209019 (cit. on p. 4).
- [12] V. Mauth, *Realization of a <sup>87</sup>Rb magneto-optical trap*, Bachelor Thesis: University of Bonn, 2023 (cit. on p. 4).
- [13] S. Germer, Frequency stabilization of a laser and a high resolution optical setup for excitation of ultracold Rydberg atoms, Bachelor Thesis: University of Bonn, 2023 (cit. on p. 4).
- [14] R. S. Quimby and R. C. Powell, "Types of Lasers", Springer Handbook of Atomic, Molecular, and Optical Physics, ed. by G. W. F. Drake, Cham: Springer International Publishing, 2023 1081, ISBN: 978-3-030-73893-8, URL: https://doi.org/10.1007/978-3-030-73893-8\_75 (cit. on p. 6).
- [15] E. D. Black, An introduction to Pound-Drever-Hall laser frequency stabilization, American Journal of Physics 69 (2001) 79, ISSN: 0002-9505, eprint: https://pubs.aip.org/aapt/ajp/article-pdf/69/1/79/10115998/79\\_1\\_online.pdf, URL: https://doi.org/10.1119/1.1286663 (cit. on pp. 6, 25).
- [16] A. Cansiz, Setting up a Rydberg excitation laser and stabilizing its frequency to an ultra-stable reference cavity, Bachelor Thesis: University of Bonn, 2025 (cit. on p. 6).
- [17] Tunable Diode Lasers, 2018, URL: https: //www.toptica.com/fileadmin/Editors\_English/11\_brochures\_ datasheets/01\_brochures/toptica\_BR\_Scientific\_Lasers.pdf (visited on 09/07/2025) (cit. on pp. 6, 7).
- [18] TA-SHG pro: High-power, tunable, frequency-doubled diode laser, 2018, URL: https://www.toptica.com/products/tunable-diode-lasers/frequency-converted-lasers/ta-shg-pro#gallery-2 (visited on 11/07/2025) (cit. on p. 6).
- [19] R. Paschotta, Frequency Doubling, RP Photonics Encyclopedia, Available online at https://www.rp-photonics.com/frequency\_doubling.html, 2006, URL: https://www.rp-photonics.com/frequency\_doubling.html (visited on 09/07/2025) (cit. on p. 7).
- [20] Understanding Waveplates and Retarders, 2025,

  URL: https://www.edmundoptics.com/knowledge-center/applicationnotes/optics/understanding-waveplates/(visited on 21/07/2025)

  (cit. on pp. 8, 13).
- [21] Broadband Polarizing Beamsplitter Cubes, 2025, URL: https://www.thorlabs.com/newgrouppage9.cfm?objectgroup\_id=739 (visited on 12/07/2025) (cit. on p. 8).

- [22] R. Paschotta, *Acousto-optic Modulators*, RP Photonics Encyclopedia, Available online at https://www.rp-photonics.com/acousto\_optic\_modulators.html, 2008,

  URL: https://www.rp-photonics.com/acousto\_optic\_modulators.html
  (visited on 12/07/2025) (cit. on p. 8).
- [23] Application Note: Acousto-Optic Frequency shifters, 2012,

  URL: https://wiki.nqo.uni-bonn.de/images/AcoustoOptic\_Frequency\_Shifters\_application\_note\_Isomet\_2012.pdf
  (visited on 12/07/2025) (cit. on p. 9).
- [24] AOMO 3080-120, 2025, URL: https://gandh.com/products/acousto-optics/modulators/aomo-3080-120 (visited on 12/07/2025) (cit. on p. 9).
- [25] R. Paschotta, *Gaussian Beams*, RP Photonics Encyclopedia,

  Available online at https://www.rp-photonics.com/gaussian\_beams.html,

  2005, URL: https://www.rp-photonics.com/gaussian\_beams.html (visited on 13/07/2025) (cit. on p. 9).
- [26] M. Araújo, R. Silva, E. Lima, D. Pereira and P. De Oliveira, *Measurement of Gaussian laser beam radius using the knife-edge technique: improvement on data analysis*, Applied Optics **48** (2009) 393 (cit. on p. 9).
- [27] M. M. Rashad, Measurements of Laser Beam Using Knife Edge Technique, URL: https://www.politesi.polimi.it/retrieve/b0b19da2-0788-434f-8313-4264bffda739/la%5C%20tesina%5C%20revised-converted.pdf (visited on 13/07/2025) (cit. on p. 10).
- [28] T. Chartier, "Optical Fibers", Springer Handbook of Glass, ed. by J. D. Musgraves, J. Hu and L. Calvez, Cham: Springer International Publishing, 2019 1405, ISBN: 978-3-319-93728-1, URL: https://doi.org/10.1007/978-3-319-93728-1\_41 (cit. on p. 13).
- [29] M. Ding, D. Fan, W. Wang, Y. Luo and G.-D. Peng, "Basics of Optical Fiber Measurements", *Handbook of Optical Fibers*, ed. by G.-D. Peng, Singapore: Springer Singapore, 2019 1099, ISBN: 978-981-10-7087-7, URL: https://doi.org/10.1007/978-981-10-7087-7\_57 (cit. on p. 13).
- [30] POLARIZATION MAINTAINING FIBER PATCHCORDS AND CONNECTORS, URL: https://shop.amstechnologies.com/media/89/e1/ac/1720718100/PMJ-QPMJ-PM-Patch-Cables-OZ-Optics-Datasheet.pdf?ts=1734635169 (visited on 17/07/2025) (cit. on pp. 13, 14).
- [31] An Overview of Polarization Extinction Ratio Measurement Methods, URL: https://lunainc.com/sites/default/files/assets/files/resource-library/PER-Measurement-Note.pdf (visited on 27/07/2025) (cit. on p. 14).
- [32] C. J. Foot, *Atomic Physics*, Oxford University Press, 2004, ISBN: 9780198506959, URL: https://doi.org/10.1093/oso/9780198506959.001.0001 (cit. on pp. 16, 21).

- [33] J. Dalibard and C. Cohen-Tannoudji,

  Laser cooling below the Doppler limit by polarization gradients: simple theoretical models,

  J. Opt. Soc. Am. B 6 (1989) 2023, URL:

  https://opg.optica.org/josab/abstract.cfm?URI=josab-6-11-2023
  (cit. on p. 16).
- [34] J. Gamper, *Atom Preparation and Rydberg Excitation of Rubidium Atoms*, Master Thesis: University of Bonn, 2024 (cit. on pp. 16, 19–21).
- [35] V. Mauth, Machine Learning based Optimization for the Preparation of Rubidium Rydberg Atoms and Characterization of the Detection, Master Thesis: University of Bonn, 2025 (cit. on p. 16).
- [36] R. W. G. Moore et al.,

  Measurement of vacuum pressure with a magneto-optical trap: A pressure-rise method,

  Review of Scientific Instruments 86 (2015) 093108, ISSN: 0034-6748,

  eprint: https://pubs.aip.org/aip/rsi/article
  pdf/doi/10.1063/1.4928154/15827205/093108\\_1\\_online.pdf,

  URL: https://doi.org/10.1063/1.4928154 (cit. on p. 16).
- [37] Single Photon Counting Modules Count-Series, URL: https://www.lasercomponents.com/fileadmin/user\_upload/home/ Datasheets/lc-photon-counter/count-series.pdf (visited on 24/07/2025) (cit. on p. 21).
- [38] M. Fleischhauer, A. Imamoglu and J. P. Marangos, Electromagnetically induced transparency: Optics in coherent media, Rev. Mod. Phys. 77 (2 2005) 633, URL: https://link.aps.org/doi/10.1103/RevModPhys.77.633 (cit. on p. 22).
- [39] L. Sadowski,

  Design of a superconducting atom chip for interfacing Rydberg atoms with microwave resonators,

  Master Thesis: University of Bonn, 2024 (cit. on p. 23).